On-chip Lock-in Detection for Ultrafast Spectroscopy of Single Particles

Subhasis Adhikari[#,1,2], Niklas Gross[#,1], Kelly S. Wilson[3], Ojasvi Verma[1,2], Zhenyang Jia[4,5], Christy F. Landes[1,2,4,5,6,7], Sean T. Roberts[3], Stephan Link[*,1,2,6,7]

[1]Department of Chemistry, University of Illinois at Urbana-Champaign, Urbana, Illinois 61801, United States

[2]Department of Chemistry, Rice University, Houston, Texas 77005, United States

[3]Department of Chemistry, The University of Texas at Austin, Austin, Texas 78712, United States

[4]Department of Chemical and Biomolecular Engineering, Rice University, Houston, Texas 77005, United States

[5]Department of Chemical and Biomolecular Engineering, University of Illinois at Urbana-Champaign, Urbana, Illinois 61801, United States

[6]Department of Electrical and Computer Engineering, Rice University, Houston, Texas 77005, United States

[7]Department of Electrical and Computer Engineering, University of Illinois at Urbana-Champaign, Urbana, Illinois 61801, United States

Keywords: Transient extinction spectroscopy, pump-probe spectroscopy, surface plasmon, acoustic vibrations, lock-in camera

Abstract

Time-resolved spectroscopy of plasmonic nanoparticles is a vital technique for probing their ultrafast electron dynamics and subsequent acoustic and photothermal properties. Traditionally, these experiments are performed with spectrally-broad probe beams on the ensemble level to achieve high signal amplitudes. However, the relaxation dynamics of plasmonic nanoparticles are highly dependent on their size, shape, and crystallinity. As such, the inherent heterogeneity of most nanoparticle samples can complicate efforts to build microscopic models for these dynamics based solely on ensemble measurements. Although approaches for collecting time-resolved microscopy signals from individual nanoparticles at selected probe wavelengths have been demonstrated, acquiring time-resolved spectra from single objects remains challenging. Here, we demonstrate an alternate method that efficiently yields time-resolved spectra of a single gold nanodisk in one measurement. By modulating the frequency-doubled output of a 96 MHz Ti:Sapphire oscillator at 8 kHz, we are able to use a lock-in pixel-array camera to detect photo-induced changes in the transmission of a white light continuum probe derived from a photonic crystal fiber to produce broadband femtosecond transmission spectra of a single gold nanodisk. We also compare the performance of the lock-in camera for the same single nanoparticle to detection with a single-element photodiode and find comparable sensitivities. The lock-in camera thus provides a major advantage due to its ability to multiplex spectral detection, which we utilize here to capture both the electronic dynamics and acoustic vibrations of a single gold nanodisk following ultrafast laser excitation.

Introduction

Single-particle spectroscopy is the basis for mechanistic studies of the optical properties of metallic and semiconducting nanomaterials.[1,2] By measuring individual particles, the dependence of the optical behavior on the distinct physical properties of each particle is taken into account, thereby eliminating spectral broadening and other effects that stem from heterogeneity within a nanoparticle ensemble.[3] Various steady-state, single-particle techniques have been developed to obtain spectral information regarding the absorption, scattering, emission, and extinction of light by nanomaterials[4–7] such as plasmonic nanoparticles,[8] carbon nanomaterials,[9] and quantum dots.[10] The gained insights have made nanomaterials promising for many applications in diverse areas such as catalysis, sensing, and photothermal therapy.[11–14]

Beyond the steady-state regime, time-resolved studies are vital to understanding the underlying mechanisms that govern the optical properties of these nanomaterials.[15–18] By tracking the optical behavior down to the femtosecond timescale after initial photoexcitation, time-resolved methods can resolve the ultrafast dynamics of photoexcited charge carriers, like their equilibration and diffusion, as well as subsequent mechanical and thermal effects.[15,19] Often employed time-resolved methods such as transient absorption/extinction spectroscopy and 2D ultrafast spectroscopy use laser pulses to pump and probe samples with adjustable time delays between them.[20] On the ensemble level, these techniques have provided a wealth of information on systems ranging from biological materials to organic crystals and nanoparticles.[21,22] However, measurements of single-particles are required to fully resolve their photoexcited dynamics if the material's properties are affected by heterogeneity in particle morphology or local environment.

Time-resolved spectroscopy of individual nanoparticles is experimentally challenging due to the difficulty of obtaining sufficient signal levels across a range of probe wavelengths.[19] To perform time-resolved measurements of nanoparticle ensembles, femtosecond laser sources, often with repetition rates in the kHz regime, are used to generate excitation pulses via optical parametric amplification and spectrally broad probe pulses via supercontinuum generation. These pulses are often loosely focused to spots of a few hundred microns to prevent photodamage and pump-induced changes in the transmission of the probe pulse can be readily detected using either a charge-coupled device (CCD) or complementary metal–oxide–semiconductor (CMOS) detector coupled to a spectrometer. In contrast, time-resolved measurements of single particles are typically performed by focusing the pump and probe pulses to diffraction-limited spots using microscope objectives to increase signal amplitude.[23–27] Despite this tight focus however, these signal levels are generally too small to be detectable using standard cameras. To address this issue, detection of pump-probe signals is often performed using pre-amplifying photodiodes or photomultipliers in combination with lock-in amplification to extract small signals from the much larger background. Use of high repetition rate lasers (>1 MHz) can further boost this detection scheme by allowing for improved signal averaging while employing low-power pulses that reduce the risk of sample photodamage.[19] However, this detection scheme comes with a trade off in the area of spectral detection as single photodiodes can only capture a single probe wavelength at a time. While spectral information for single nanoparticles can be achieved by performing multiple measurements at different, individual wavelengths in a sequential manner,[28,29] data collection via this scheme is time-consuming and can be impacted by fluctuations in the spectral profile of the probe source. New methods are desperately needed to advance the ultrafast spectroscopy of single nanoparticles.

To address this challenge, we have integrated a pixel-array lock-in camera into a time-resolved transient transmission microscope and have used it measure the transient transmission spectrum of an individual gold nanodisk (AuND) in a single measurement. Each pixel of the lock-in camera behaves similarly to a photodiode coupled to a lock-in amplifier, allowing for high-sensitivity detection of the transient extinction signal for a spectrally dispersed probe beam. To the best of our knowledge, pixel-array lock-in cameras have only been used on bulk materials such as diamond powder, but not on single nanoparticles.[30] We first demonstrate that the lock-in camera is capable of measuring the transient transmission signal of a single AuND. We validate this result by comparing it to a measurement performed on the same AuND using the previously described and well-established photodiode detection method.[31] Finally, we show that the approach utilizing the lock-in camera introduced here yields a time-resolved transient spectrum for a single AuND in one measurement, thereby allowing us to access both the electronic dynamics and acoustic vibrations of the AuND at several wavelengths simultaneously.

Experimental Methods

2 × 2 arrays of AuNDs with diameters of 120 nm and 140 nm, a thickness of 35 nm, and an interparticle distance of 10 μm were fabricated using electron beam lithography (EBL) on glass. 25 × 25 × 0.17 mm glass substrates (Corning, Product Number 2850-25) were cleaned by washing in an ultrasonic bath with a 2% (v/v) Hellmanex detergent, 200 proof ethanol, and ultrapure water for 10 minutes each. Subsequently, the substrates were dried under a stream of nitrogen and plasma etched with oxygen for 2 minutes. The substrates were then spin-coated at 4000 rpm for 1 minute with 950 poly (methyl methacrylate) A4 (Kayaku Advanced Materials),

followed by a 2-minute bake on a 180 °C hotplate. Afterward, the coverslips were spin-coated with the conductive polymer Espacer 300Z (Showa Denko) at 3000 rpm for 1 minute and taken to an Elionix ELS-G100 electron beam writer operating at 100 kV and 1 nA. The patterns were developed by immersion for 65 s in a 1:3 (v/v) solution of methyl isobutyl ketone:isopropyl alcohol (MIBK:IPA), followed by a rinse in IPA before being gently blown dry with nitrogen. Metal layers were deposited at a rate of 0.3 Å/s using an electron beam evaporator, starting with a 2 nm Ti adhesion layer, followed by a 35 nm Au deposition. Finally, excess Au and Ti were removed by soaking the samples in acetone for 72 hours, followed by gentle sonication and drying under a nitrogen stream.

The AuND arrays were characterized by scanning electron microscopy (SEM) on an FEI Quanta 400 ESEM FEG using a dwell time of 10 μs and a voltage of 15 kV. Due to the non-conductive nature of the glass substrates, all images were measured under environmental conditions in a water atmosphere at ~4×10^{-4} Torr.

Single-particle dark-field scattering (DFS) spectra were recorded using a home-built inverted dark-field microscopy setup based on a Zeiss microscope (Axio Observer m1, with oil immersion condenser, numerical aperture NA = 0.7 – 1.4). The scattered light by a nanoparticle was collected through an oil immersion microscope objective (Zeiss Plan-Achromat 63×, NA = 0.7 – 1.4) and directed to an imaging spectrograph (Princeton Instruments Acton SpectraPro 2150i with thermoelectrically cooled back-illuminated CCD camera, Princeton Instruments PIXIS 400BR) mounted on a linear translation stage to record scattering spectra of multiple nanoparticles in a hyperspectral configuration.[32]

Results and Discussion

Single-particle transient transmission imaging and spectroscopy were performed using a homebuilt setup, as illustrated in Figure 1A. A 7 W, 532 nm continuous-wave laser (Coherent Verdi G10) was used to pump a Ti:sapphire oscillator (KMLabs Griffin-10), producing ~100 fs pulses at a repetition rate of 96 MHz and a center wavelength of 800 nm. The fundamental 800 nm output was split into two parts; one that was frequency doubled to 400 nm by second harmonic generation in a beta barium borate crystal (Altos BBO-1004H), while the other was directed into a non-linear photonic crystal fiber (NKT Photonics FemtoWHITE 800) to produce a white light continuum with a wavelength range starting around 550 nm for the highest pump powers and extending beyond the sensitivities of the silicon-based detectors used here. The 400 nm beam was used as the pump to excite Au interband transitions.[33] For the probe beam, we utilized the portion of the white light continuum in the range of 550 – 800 nm, as well as the fundamental 800 nm beam for comparison because of its higher intensity stability. Longer wavelengths than 800 nm of the white light continuum were eliminated through short-pass filters. An optical delay stage (Newport UTS150CC) in the probe beam path controlled the temporal overlap of the pump and probe pulses, and the pump was modulated with an optical chopper (Newport Model 3502) at 8 kHz. The pump and probe beams were recombined with a dichroic mirror and an oil immersion objective (Zeiss Plan-Apochromat 63×, 1.4 NA) focused the beams on the sample. The light was collected by a receiving objective (Zeiss LD Achroplan 40×, 0.6 NA) in a transmission geometry, while long-pass filters removed the pump before detection of the probe. The beam energy densities at the sample were approximately 4.38×10^4 W/cm^2 for the pump, 1.4×10^5 W/cm^2 for the white light continuum probe, and 0.7×10^5 W/cm^2 for the 800 nm fundamental probe, considering beam sizes measured by the knife-edge method

varying between 250 to 500 nm (Figure S1). Detection could be alternated for the same AuND between using either a standard single-element photodiode or the lock-in camera.

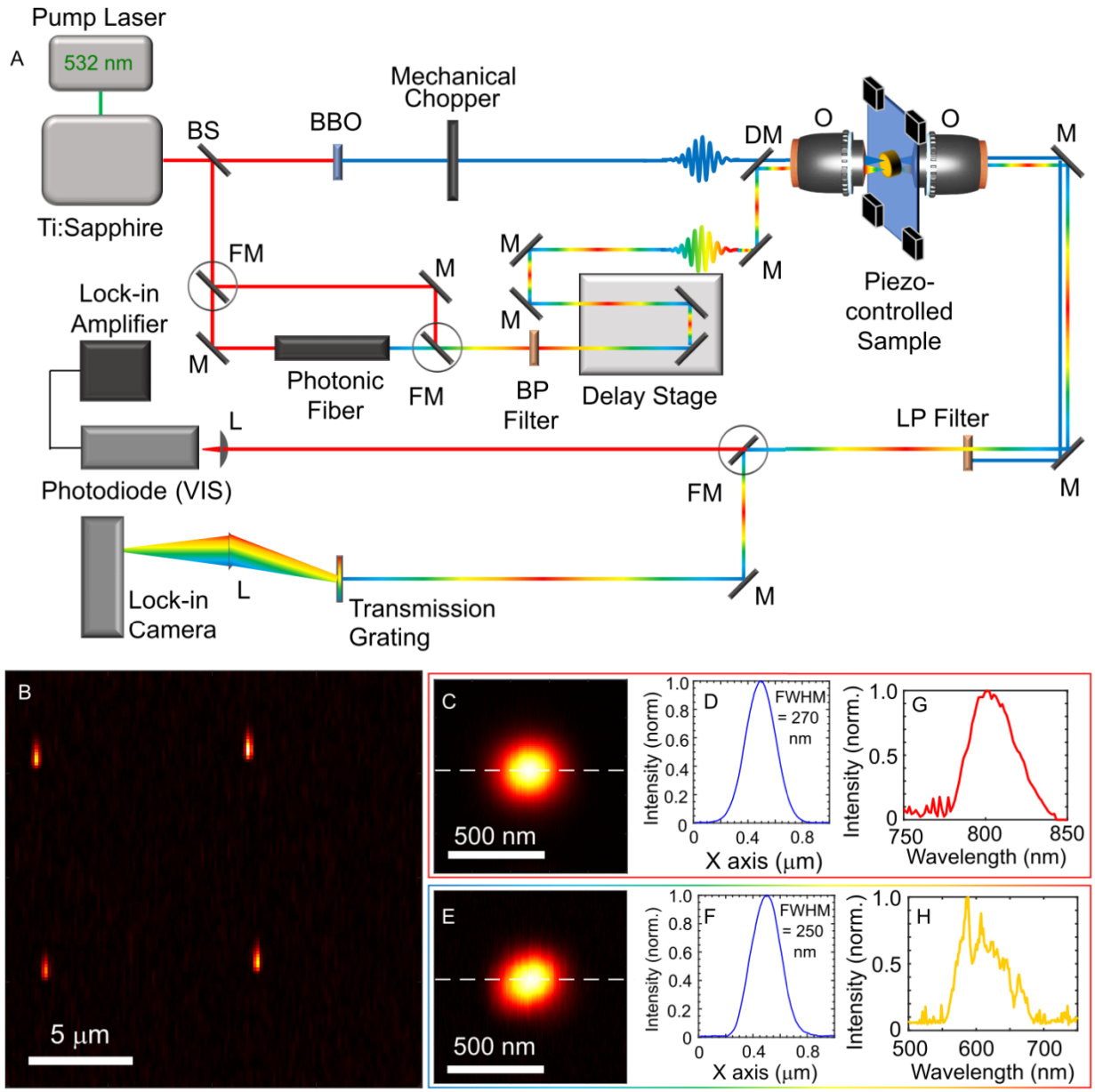

Figure 1: (A) Schematic of the optical setup. See text for details. Red line: 800 nm probe; blue line: 400 nm pump; rainbow colored line: white light continuum probe. BS: beam-splitter; BBO: beta barium borate crystal; FM: flip mirror; M: mirror; DM: dichroic mirror; O: objective; BP:

band-pass filter; LP: long-pass filter; L: lens. Note that pump and probe beam paths are spatially displaced for visualization only. (B) 20 µm × 20 µm transient transmission image of a 2 × 2 array containing 120 (left) and 140 (right) nm AuNDs using 400 nm pump and 800 nm probe. The elongated shape of the point spread function is an artifact due to fast scanning along the vertical direction, as seen from the magnified 1 × 1 µm image of a single 120 nm AuND (C). The corresponding line profile is given in (D) and yields a FWHM of about 270 nm. (E) 1 × 1 µm image of a 120 nm disk using the entire white light continuum as a probe. The corresponding line profile is given in (F) and yields a FWHM of about 250 nm. All intensities in (B) - (F) were normalized. (G) Typical spectrum of the 800 nm probe. (H) An example spectrum of the white light continuum probe. Note that the spectral width can be increased by boosting the 800 nm laser power sent into the photonic fiber. However, this narrower spectral width was chosen for the data in Figure 4 to minimize intensity fluctuations.

With this setup we achieved diffraction-limited imaging of individual AuNDs (Figure 1B). AuNDs were visualized in transient transmission images by raster-scanning the sample with a piezo nanopositioning stage (Physik Instrumente P-517.3CL), while spatially and temporally overlapping the confocal pump and probe beams. Figure 1B shows an exemplary transient transmission image of a 2 × 2 array containing 120 (left column) and 140 (right column) nm AuNDs. To better characterize the point spread function, Figure 1C illustrates a raster-scanned image of only a single 120 nm disk using 400 and 800 nm as the pump and probe beam, respectively. A line profile along the horizontal axis at the maximum signal (Figure 1D) reveals a full width at half maximum (FWHM) of about 270 nm, consistent with diffraction-limited resolution. The corresponding image and line section when using the entire white light continuum probe are given in Figures 1E and 1F. In this case, we determined a FWHM of about

250 nm, which, considering a peak probe wavelength near 650 nm, is again in agreement with diffraction-limited imaging.

For transient transmission imaging, as shown in Figures 1B-D, we employed a photodiode (Femto DHPCA-100-F) that was connected to a lock-in amplifier (Zurich Instruments UHFLI). The lock-in amplifier demodulated the signal using the frequency of the pump beam modulation as a reference input, yielding as output the pump-induced transmitted signal ΔT. ΔT was digitized with a data acquisition board (National Instruments USB-6229), collected with a custom LabVIEW program, and processed using MATLAB. To determine the reference transmission signal with the pump off, the signal from the photodiode was referenced simultaneously to the laser repetition rate, allowing for real-time normalization and thus recording of the normalized differential transient transmission $\Delta T/T$.

In contrast, for transient transmission spectroscopy of individual AuNDs, we designed and implemented a spectrometer based on a transmission grating with a groove density of 300/mm and a blaze angle of 17.5° (Edmund Optics Article #49579) to spectrally disperse the probe beam onto a pixel-array lock-in camera (Heliotis heliCam C3). A lens with a focal length of 100 mm was placed between the transmission grating and the lock-in camera. The camera consists of an array of 300 × 300 pixels that each offer lock-in capabilities and analog-to-digital conversion. By spreading the spectrum across the pixel array, it is thus possible to acquire ΔT over multiple wavelengths simultaneously using a high repetition rate femtosecond oscillator. To extract the transient transmission signal, the pump modulation frequency of 8 kHz was synchronized with the lock-in camera. The transient transmission spectra were processed using the same LabVIEW program and analyzed in MATLAB. Wavelength calibration and correction for temporal chirp of the probe beam are described in Figure S2. Each acquired frame was collected by integrating

over 160 cycles, and the final output signal was averaged over 80 frames to achieve a high signal-to-noise ratio (SNR). While further increasing the number of collected cycles or frames is limited by the camera memory, additional post-acquisition averaging offers a pathway to even higher SNRs, but was not needed for these studies. The lock-in camera can also be operated in an intensity mode to obtain transmission spectra without the pump. These spectra were used to correct for the intensity profile of the probe beam. Example spectral profiles of the fundamental 800 nm and white light continuum probe pulses are given in Figures 1G and 1H.

To compare the performance of the lock-in camera with the single-element photodiode, we first performed transient transmission measurements of a 140 nm AuND, using 800 nm as the probe. The DFS spectrum and SEM image of the selected AuND are given in Figure 2A. SEM analysis confirmed a diameter of 137 nm, close to the size expected based on the sample design. As the DFS spectrum peaks at 700 nm, the 800 nm probe beam reports on dynamics at the lower energy wing of the plasmon resonance. Figure 2B presents the $\Delta T/T$ time transient recorded with the photodiode by positioning a single AuND at the focus of the overlapped pump and probe beams and scanning the time delay separating them. Consistent with previous transient transmission measurements of single AuNDs,[3,31] the data shows an instrument-limited fast rise in induced transmission caused by plasmon bleaching in response to creation of a hot electron distribution followed by a picosecond decay of this signal due to electron-phonon coupling and subsequent slower thermal equilibration with the supporting substrate.

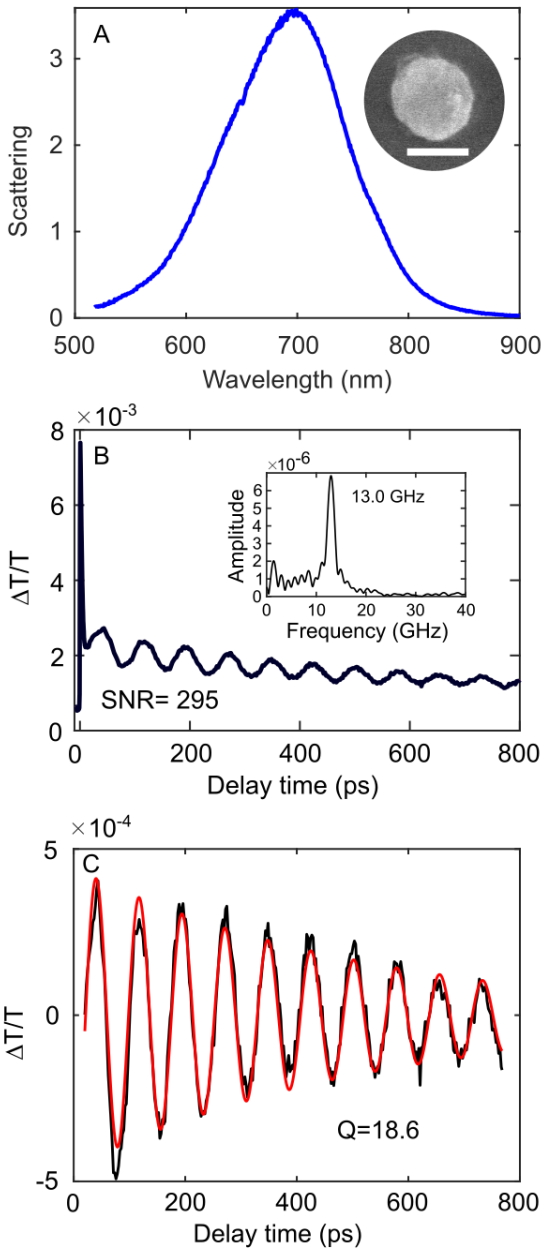

Figure 2: (A) DFS spectrum of a 140 nm AuND with its corresponding SEM image given in the inset (scale bar = 100 nm). (B) Time-dependent transient transmission of the same AuND, measured with an integration time per delay step of 600 ms. The SNR was calculated as the maximum signal subtracted by the offset signal before zero delay time and normalized by the standard deviation of the offset signal. Inset: Power spectrum obtained by Fourier transform of

the oscillatory part of the transient transmission, yielding an acoustic mode frequency of 13.0 GHz. (C) Acoustic oscillation signal isolated from the data in B by subtraction of an exponential fit (black). This signal was fit to a damped exponential decay (Eq. 1, red).

To compare this transient with one recorded using the lock-in camera, we first focus on the latter decay component, which is modulated due to the excitation of acoustic modes by impulsive heating when the electrons couple to the metal's phonon bath. These acoustic oscillations were isolated as the residuals of the time transient after subtraction of an exponential decay that was fit to the data considering only delay times longer than 20 ps. These oscillations can be described by a quality factor Q defined as $Q = \pi\tau\nu$, where ν is the oscillation frequency and τ is the damping time. Figure 2C highlights the acoustic mode of a single 140 nm AuND (black) and a fit (red) using a damped cosine function according to:

$$\frac{\Delta T}{T}(t) \sim exp\left(-\frac{t}{\tau}\right) \times cos(2\pi\nu t + \varphi) \qquad \text{Eq. 1}$$

Here, t is the delay time between the pump and probe and φ represents the oscillation phase. The oscillation frequency, most easily extracted from the Fourier transform of the acoustic oscillations (Figure 2B inset), was found to be 13.0 GHz, while the cosine function fit resulted in a damping time of 456 ps. Thus, the quality factor was 18.6, in good agreement with our previous work,[31] where further experimental and analysis details can be found.

Lock-in camera detection for the same single 140 nm AuND under identical excitation conditions while spectrally dispersing the 800 nm probe yielded a very similar quality factor and overall performance. Figure 3A displays wavelength-resolved transient transmission dynamics of the AuND collected following 400 nm excitation. The acoustic mode is clearly seen in the time-

dependent transient spectra, and although the lock-in camera provides the additional benefit of spectral information compared to the photodiode, here we focus first on comparing the sensitivities of the two detectors at a single wavelength. For such direct comparison, the transient transmission in Figure 3A was averaged over the whole spectral width of the 800 nm fundamental (Figure 3B) and the oscillatory component was isolated (Figure 3C), as described above. Fitting to Eq. 1 and Fourier transforming the data gave a frequency of 12.9 GHz and a damping time of 381 ps, from which we calculated a Q-factor of 15.5, in good agreement with the results obtained for the single-element photodiode (Figure 2). Comparing now the SNRs for the traces in Figures 2B and 3B, we determined values of 295 and 185, respectively. However, the integration times differed; 0.6 s and 3.2 s per delay step were used for the photodiode and lock-in camera, respectively. Considering SNR and integration time, the sensitivity (i.e., SNR/√integration time) for lock-in camera detection is about a factor of 3.7 smaller than that of the photodiode. Integrating over only a 20 nm spectral slide of the probe pulses centered at 800 nm, this factor drops only slightly to 4.5. While the lock-in camera's sensitivity is slightly lower than that of the photodiode, we note that it is more than sufficient to record high-quality, spectrally-resolved pump-probe measurements, such as single-particle transient absorption and photothermal spectroscopy and microscopy.[4,7]

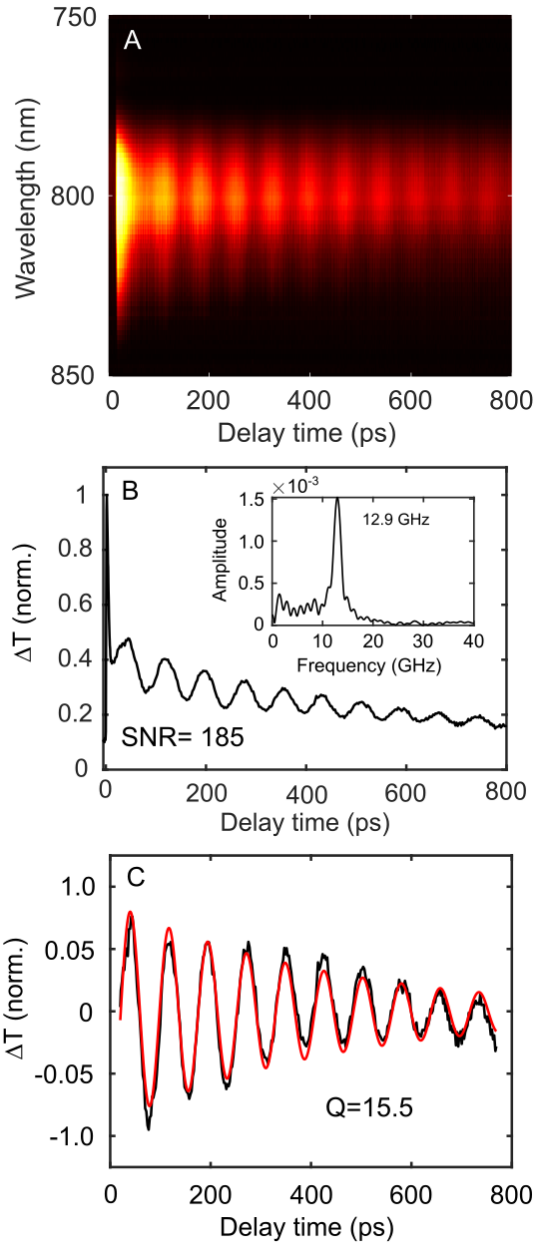

Figure 3: (A) Transient transmission spectra of the same AuND as shown in Figure 2, measured with the lock-in camera using 400 nm and 800 nm pulses as the pump and probe, respectively. (B) Transient transmission generated from spectra in (A) by integrating over the whole spectral width of the 800 nm probe at each pump-probe delay time. The integration time per delay step was 3.2 s. Inset: Power spectrum obtained by Fourier transform of the oscillatory part of the

transient transmission, yielding an acoustic mode frequency of 12.9 GHz. (C) Acoustic oscillation signal isolated from the data in B by subtraction of an exponential fit (black). This signal was fit to a damped exponential decay (Eq. 1, red).

Switching to the white light continuum probe allowed us to measure an entire transient transmission spectrum of a single nanoparticle using the combination of the lock-in camera and a high repetition rate femtosecond oscillator, resolving both the initial electron relaxation dynamics and acoustic vibrations of a single 120 nm AuND (Figure 4). Figure 4A shows transient transmission spectra of the single AuND as a function of pump-probe delay time. These spectra were corrected for wavelength-dependent variations in the probe intensity and camera quantum efficiency, probe pulse chirp (Figure S2), and a static background signal that was removed by subtracting the signal measured at negative pump-probe time delays from each wavelength channel. The maximum transient transmission is seen between 650 nm and 700 nm, which falls near the peak of the plasmon resonance of the 120 nm AuND, as confirmed by the corresponding DFS spectrum (Figure S3). The single-particle transient transmission spectrum of the 120 nm AuND is given in Figure 4B and was averaged over the initial electron-phonon relaxation dynamics from 1 to 5 ps, while considering the phase as obtained for different probe wavelengths using the lock-in amplifier (Figure S4). In excellent agreement with many previous ensemble transient extinction measurements,[4,34,35] we see a photoinduced bleach near the peak of the localized surface plasmon resonance and induced absorption at the wings. This lineshape results from spectral broadening of the plasmon due to an elevation of the nanoparticle's electronic temperature following light absorption. Finally, we note that the sharper features of the single-particle transient transmission spectrum arise from fluctuations of the white light

continuum. Future improvements in its stability together with an enhanced algorithm for probe intensity correction will address this issue.

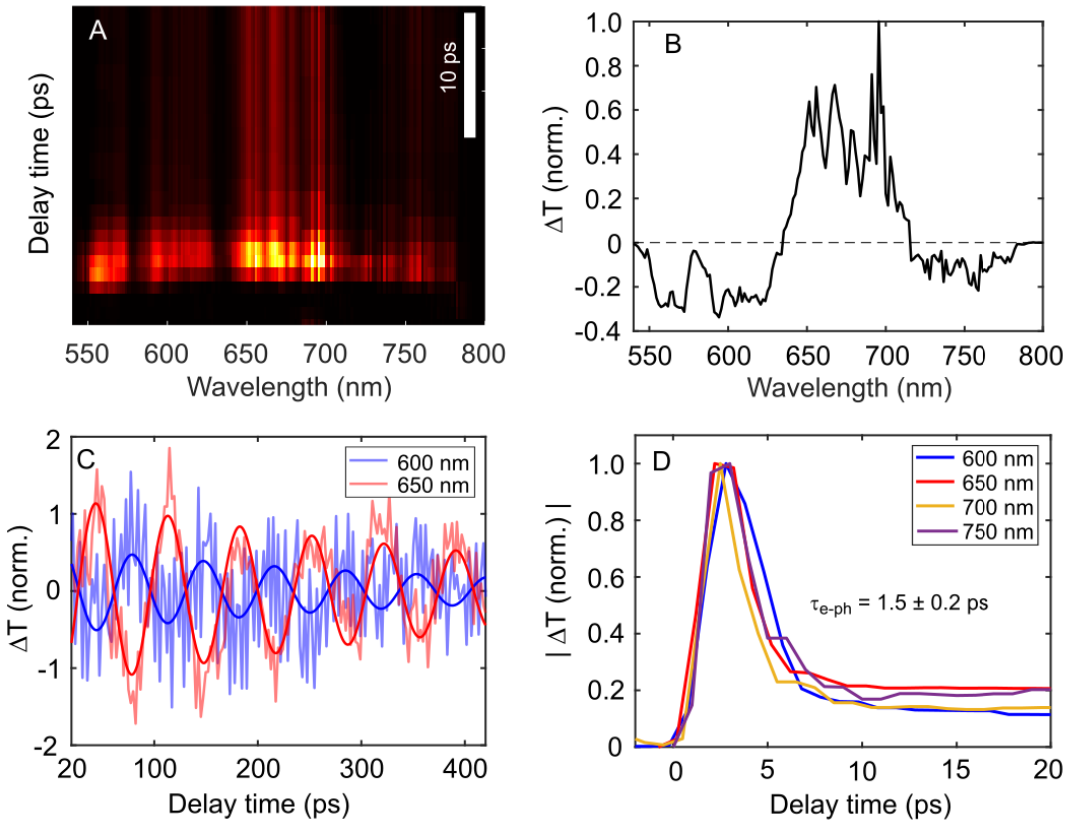

Figure 4: (A) Time-resolved transient transmission of a single 120 nm AuND using a white light continuum as the probe and the lock-in camera as the detector. The signal was corrected for pulse chirp and a background, pre-time zero offset. (B) Transient transmission spectrum averaged over pump-probe delay times of 1 to 5 ps, as extracted from the data in (A), considering also the signal phase, as incorporated from Figure S4. (C) Acoustic oscillations with fits to Eq. 1 for two different probe wavelengths with centers at 600 nm and 650 nm, averaged over spectral windows of 20 nm. The oscillations are out of phase, consistent with the change in the sign of the transient transmission observed in (B). (D) Short-time ultrafast transient dynamics that probe electron-phonon relaxation, simultaneously measured at four different

probe wavelengths. Each data trace was constructed by averaging the transient transmission in (A) over a spectral window of 20 nm centered at each listed probe wavelength. An exponential fit (not shown for clarity) yields an electron-phonon relaxation time of $\tau_{e\text{-}ph} = 1.5 \pm 0.2$ *ps. The integration time per delay step was 3.2 seconds.*

In addition to spectral information, a main advantage of the lock-in camera setup is that the dynamics at different wavelengths are instantly available, as illustrated for the acoustic vibrations (Figure 4C) and electron-phonon relaxation (Figure 4D) of the 120 nm AuND. The acoustic oscillations at 600 nm and 650 nm, analyzed as described above, were found to be out-of-phase, with similar oscillation frequencies of 14.5 GHz and 14.4 GHz, respectively (Figure 4C). These results are consistent with the phase change observed in the transient transmission spectrum, caused by a periodic plasmon resonance shift due to the changes in particle volume induced by the acoustic breathing mode.[36] Using the 800 nm fundamental as the probe because of its higher stability and hence increased SNR, confirms an oscillation frequency of 14.2 GHz for another 120 AuND (Figure S4). Shifting our focus to the initial 20 ps pump-probe delay times, Figure 4D illustrates that both the plasmon bleach and induced absorptions at shorter and longer probe wavelengths have the same decay times. This observation that the electron-phonon relaxation is independent of probe wavelength reflects the cooling of the hot electron distribution that gives rise to transient plasmon damping. These results are consistent with ensemble transient absorption spectroscopy of gold nanospheres, where it was found that the measured electron-phonon relaxation time depends only on the rise in electron temperature.[4,35]

Despite a slightly lower sensitivity compared to a single-element detector, the lock-in camera provides a key advantage by enabling the simultaneous recording of time-resolved dynamics over a broad wavelength range of several hundred nanometers. Instead of just imaging at a fixed

wavelength, our results demonstrate the impressive potential of the lock-in camera by illustrating how spectroscopy of single nanoparticles is now possible with MHz repetition rate ultrafast lasers. Note that, even though the lock-in camera has a two-dimensional pixel array, we have here used only one line of pixels. Future implementation of full-chip lock-in imaging would allow spectroscopy of multiple nanoparticles simultaneously, similar to hyperspectral imaging. Further improvements in the stability of the white light continuum and its real-time correction, as well as direct measurement of phase information, will further expand the capabilities of the lock-in camera for single-particle ultrafast spectroscopy. Finally, although we have demonstrated here the implementation of a lock-in camera specifically for single-particle transient extinction spectroscopy, it can in principle be applied to any single-particle pump-probe modulation spectroscopy or wide-field imaging.

Conclusions

We implemented a pixel-array lock-in camera into a time-resolved transient transmission microscope and showcased its ability to efficiently measure the temporally and spectrally resolved ultrafast dynamics of single nanoparticles. Using lithographically-prepared single AuNDs as a test sample, we introduced the required experimental instrumentation and corresponding calibration and normalization procedures to acquire time-resolved single-particle spectra. The acquired spectra display broadening of the plasmon lineshape following ultrafast excitation, resulting in bleaching near the peak of the plasmon resonance and induced absorption at its edges. We also illustrated that the lock-in camera can resolve coherent acoustic vibrations of single nanoparticles. We found that the sensitivity and SNR of the lock-in camera approaches

that produced by performing lock-in detection with a single-element photodiode while simultaneously allowing for multiplexed spectral detection of transient transmission signals. As such, we anticipate lock-in camera technology has the potential to make single-nanoparticle pump-probe spectroscopy easily accessible by eliminating the need to perform slow wavelength-by-wavelength sequential scanning to acquire transient spectra.

ASSOCIATED CONTENT

Supporting Information. Beam size determination using knife-edge method, wavelength calibration and chirp correction, dark-field spectroscopy and transient transmission measurements of a single 120 nm AuND, phase measurements at different probe wavelengths.

AUTHOR INFORMATION

Corresponding Author

*slink@illinois.edu

Author Contributions

S.A. and N.G. contributed equally. All authors have given approval to the final version of the manuscript.

Notes

The authors declare no competing financial interest.

ACKNOWLEDGMENT

This work was primarily funded by the National Science Foundation, Center for Adopting Flaws as Features (CHE-2413590). S.L. thanks the Robert A. Welch Foundation (C-0002) and the National Science Foundation (DMR-2225592) for partial support. C.F.L and S.T.R. acknowledge funding from the Robert A. Welch Foundation (C-1787 & F-1885, respectively).

ABBREVIATIONS

Au: gold, Ti: titanium, AuND: gold nanodisk, CCD: charge-coupled device, CMOS: complementary metal–oxide–semiconductor, EBL: Electron beam lithography, MIBK: methyl isobutyl ketone, IPA: iso-propyl alcohol, BBO: beta barium borate, SEM: scanning electron microscopy, NA: numerical aperture, FWHM: full width half maximum, SNR: signal-to-noise ratio, Q-factor: quality factor.

REFERENCES

(1) Hartland, G. V. Ultrafast Studies of Single Semiconductor and Metal Nanostructures through Transient Absorption Microscopy. *Chem. Sci.* **2010**, *1* (3), 303–309. https://doi.org/10.1039/C0SC00243G.

(2) Zhao, T.; Herbert, P. J.; Zheng, H.; Knappenberger, K. L. Jr. State-Resolved Metal Nanoparticle Dynamics Viewed through the Combined Lenses of Ultrafast and Magneto-Optical Spectroscopies. *Acc. Chem. Res.* **2018**, *51* (6), 1433–1442. https://doi.org/10.1021/acs.accounts.8b00096.

(3) Su, M.-N.; Ostovar, B.; Gross, N.; Sader, J. E.; Chang, W.-S.; Link, S. Acoustic Vibrations and Energy Dissipation Mechanisms for Lithographically Fabricated Plasmonic Nanostructures Revealed by Single-Particle Transient Extinction Spectroscopy. *J. Phys. Chem. C* **2021**, *125* (3), 1621–1636. https://doi.org/10.1021/acs.jpcc.0c09782.

(4) Hartland, G. V. Optical Studies of Dynamics in Noble Metal Nanostructures. *Chem. Rev.* **2011**, *111* (6), 3858–3887. https://doi.org/10.1021/cr1002547.

(5) Zhou, J.; Chizhik, A. I.; Chu, S.; Jin, D. Single-Particle Spectroscopy for Functional Nanomaterials. *Nature* **2020**, *579* (7797), 41–50. https://doi.org/10.1038/s41586-020-2048-8.

(6) Peng, Y.; Xiong, B.; Peng, L.; Li, H.; He, Y.; Yeung, E. S. Recent Advances in Optical Imaging with Anisotropic Plasmonic Nanoparticles. *Anal. Chem.* **2015**, *87* (1), 200–215. https://doi.org/10.1021/ac504061p.

(7) Adhikari, S.; Spaeth, P.; Kar, A.; Baaske, M. D.; Khatua, S.; Orrit, M. Photothermal Microscopy: Imaging the Optical Absorption of Single Nanoparticles and Single Molecules. *ACS Nano* **2020**, *14* (12), 16414–16445. https://doi.org/10.1021/acsnano.0c07638.

(8) Foerster, B.; Hartelt, M.; Collins, S. S. E.; Aeschlimann, M.; Link, S.; Sönnichsen, C. Interfacial States Cause Equal Decay of Plasmons and Hot Electrons at Gold–Metal Oxide Interfaces. *Nano Lett.* **2020**, *20* (5), 3338–3343. https://doi.org/10.1021/acs.nanolett.0c00223.

(9) Xu, Q.; Zhou, Q.; Hua, Z.; Xue, Q.; Zhang, C.; Wang, X.; Pan, D.; Xiao, M. Single-Particle Spectroscopic Measurements of Fluorescent Graphene Quantum Dots. *ACS Nano* **2013**, *7* (12), 10654–10661. https://doi.org/10.1021/nn4053342.

(10) Reid, K. R.; McBride, J. R.; Freymeyer, N. J.; Thal, L. B.; Rosenthal, S. J. Chemical Structure, Ensemble and Single-Particle Spectroscopy of Thick-Shell InP–ZnSe Quantum Dots. *Nano Lett.* **2018**, *18* (2), 709–716. https://doi.org/10.1021/acs.nanolett.7b03703.

(11) Lou, M.; Bao, J. L.; Zhou, L.; Naidu, G. N.; Robatjazi, H.; Bayles, A. I.; Everitt, H. O.; Nordlander, P.; Carter, E. A.; Halas, N. J. Direct H2S Decomposition by Plasmonic Photocatalysis: Efficient Remediation plus Sustainable Hydrogen Production. *ACS Energy Lett.* **2022**, *7* (10), 3666–3674. https://doi.org/10.1021/acsenergylett.2c01755.

(12) Huang, X.; El-Sayed, I. H.; Qian, W.; El-Sayed, M. A. Cancer Cell Imaging and Photothermal Therapy in the Near-Infrared Region by Using Gold Nanorods. *J. Am. Chem. Soc.* **2006**, *128* (6), 2115–2120. https://doi.org/10.1021/ja057254a.

(13) Dacosta Fernandes, B.; Spuch-Calvar, M.; Baida, H.; Tréguer-Delapierre, M.; Oberlé, J.; Langot, P.; Burgin, J. Acoustic Vibrations of Au Nano-Bipyramids and Their Modification under Ag Deposition: A Perspective for the Development of Nanobalances. *ACS Nano* **2013**, *7* (9), 7630–7639. https://doi.org/10.1021/nn402076m.

(14) Foerster, B.; Rutten, J.; Pham, H.; Link, S.; Sönnichsen, C. Particle Plasmons as Dipole Antennas: State Representation of Relative Observables. *J. Phys. Chem. C* **2018**, *122* (33), 19116–19123. https://doi.org/10.1021/acs.jpcc.8b06350.

(15) Beane, G.; Devkota, T.; Brown, B. S.; Hartland, G. V. Ultrafast Measurements of the Dynamics of Single Nanostructures: A Review. *Rep. Prog. Phys.* **2018**, *82* (1), 016401. https://doi.org/10.1088/1361-6633/aaea4b.
(16) Kuhs, C. T.; Luther, B. M.; Krummel, A. T. Recent Advances in 2D IR Spectroscopy Driven by Advances in Ultrafast Technology. *IEEE J. Sel. Top. Quantum Electron.* **2019**, *25* (4), 1–13. https://doi.org/10.1109/JSTQE.2019.2900597.
(17) Liao, B.; Najafi, E. Scanning Ultrafast Electron Microscopy: A Novel Technique to Probe Photocarrier Dynamics with High Spatial and Temporal Resolutions. *Mater. Today Phys.* **2017**, *2*, 46–53. https://doi.org/10.1016/j.mtphys.2017.07.003.
(18) Dowgiallo, A.-M.; Schwartzberg, A. M.; Knappenberger, K. L. Jr. Structure-Dependent Coherent Acoustic Vibrations of Hollow Gold Nanospheres. *Nano Lett.* **2011**, *11* (8), 3258–3262. https://doi.org/10.1021/nl201557s.
(19) Gross, N.; Kuhs, C. T.; Ostovar, B.; Chiang, W.-Y.; Wilson, K. S.; Volek, T. S.; Faitz, Z. M.; Carlin, C. C.; Dionne, J. A.; Zanni, M. T.; Gruebele, M.; Roberts, S. T.; Link, S.; Landes, C. F. Progress and Prospects in Optical Ultrafast Microscopy in the Visible Spectral Region: Transient Absorption and Two-Dimensional Microscopy. *J. Phys. Chem. C* **2023**, *127* (30), 14557–14586. https://doi.org/10.1021/acs.jpcc.3c02091.
(20) Shim, S.-H.; Zanni, M. T. How to Turn Your Pump–Probe Instrument into a Multidimensional Spectrometer: 2D IR and Vis Spectroscopiesvia Pulse Shaping. *Phys. Chem. Chem. Phys.* **2009**, *11* (5), 748–761. https://doi.org/10.1039/B813817F.
(21) Maiuri, M.; Garavelli, M.; Cerullo, G. Ultrafast Spectroscopy: State of the Art and Open Challenges. *J. Am. Chem. Soc.* **2020**, *142* (1), 3–15. https://doi.org/10.1021/jacs.9b10533.
(22) Soavi, G.; Tempra, I.; Pantano, M. F.; Cattoni, A.; Collin, S.; Biagioni, P.; Pugno, N. M.; Cerullo, G. Ultrasensitive Characterization of Mechanical Oscillations and Plasmon Energy Shift in Gold Nanorods. *ACS Nano* **2016**, *10* (2), 2251–2258. https://doi.org/10.1021/acsnano.5b06904.
(23) Yu, K.; Sader, J. E.; Zijlstra, P.; Hong, M.; Xu, Q.-H.; Orrit, M. Probing Silver Deposition on Single Gold Nanorods by Their Acoustic Vibrations. *Nano Lett.* **2014**, *14* (2), 915–922. https://doi.org/10.1021/nl404304h.
(24) Ostovar, B.; Su, M.-N.; Renard, D.; Clark, B. D.; Dongare, P. D.; Dutta, C.; Gross, N.; Sader, J. E.; Landes, C. F.; Chang, W.-S.; Halas, N. J.; Link, S. Acoustic Vibrations of Al Nanocrystals: Size, Shape, and Crystallinity Revealed by Single-Particle Transient Extinction Spectroscopy. *J. Phys. Chem. A* **2020**, *124* (19), 3924–3934. https://doi.org/10.1021/acs.jpca.0c01190.
(25) Devkota, T.; Yu, K.; Hartland, G. V. Mass Loading Effects in the Acoustic Vibrations of Gold Nanoplates. *Nanoscale* **2019**, *11* (35), 16208–16213. https://doi.org/10.1039/C9NR05940G.
(26) Medeghini, F.; Crut, A.; Gandolfi, M.; Rossella, F.; Maioli, P.; Vallée, F.; Banfi, F.; Del Fatti, N. Controlling the Quality Factor of a Single Acoustic Nanoresonator by Tuning Its Morphology. *Nano Lett.* **2018**, *18* (8), 5159–5166. https://doi.org/10.1021/acs.nanolett.8b02096.
(27) Boggiano, H. D.; Berté, R.; Scarpettini, A. F.; Cortés, E.; Maier, S. A.; Bragas, A. V. Determination of Nanoscale Mechanical Properties of Polymers via Plasmonic Nanoantennas. *ACS Photonics* **2020**, *7* (6), 1403–1409. https://doi.org/10.1021/acsphotonics.0c00631.
(28) Su, M.-N.; Ciccarino, C. J.; Kumar, S.; Dongare, P. D.; Hosseini Jebeli, S. A.; Renard, D.; Zhang, Y.; Ostovar, B.; Chang, W.-S.; Nordlander, P.; Halas, N. J.; Sundararaman, R.; Narang,

P.; Link, S. Ultrafast Electron Dynamics in Single Aluminum Nanostructures. *Nano Lett.* **2019**, *19* (5), 3091–3097. https://doi.org/10.1021/acs.nanolett.9b00503.
(29) Rouxel, R.; Diego, M.; Maioli, P.; Lascoux, N.; Vialla, F.; Rossella, F.; Banfi, F.; Vallée, F.; Del Fatti, N.; Crut, A. Electron and Lattice Heating Contributions to the Transient Optical Response of a Single Plasmonic Nano-Object. *J. Phys. Chem. C* **2021**, *125* (42), 23275–23286. https://doi.org/10.1021/acs.jpcc.1c06629.
(30) Bonati, C.; Fay, V.; Dornier, R.; Loterie, D.; Moser, C. Lock-in Raman Difference Spectroscopy. *Opt. Express* **2022**, *30* (16), 28601–28613. https://doi.org/10.1364/OE.461246.
(31) Gross, N.; Madadi, M.; Ostovar, B.; Dongare, P. D.; McCarthy, L. A.; Chiang, W.-Y.; Chang, W.-S.; Halas, N. J.; Landes, C. F.; Sader, J. E.; Link, S. Strong Substrate Binding Modulates the Acoustic Quality Factors in Gold Nanodisks. *J. Phys. Chem. C* **2023**, *127* (10), 5054–5066. https://doi.org/10.1021/acs.jpcc.2c09099.
(32) Byers, C. P.; Hoener, B. S.; Chang, W.-S.; Yorulmaz, M.; Link, S.; Landes, C. F. Single-Particle Spectroscopy Reveals Heterogeneity in Electrochemical Tuning of the Localized Surface Plasmon. *J. Phys. Chem. B* **2014**, *118* (49), 14047–14055. https://doi.org/10.1021/jp504454y.
(33) Zhang, X.; Huang, C.; Wang, M.; Huang, P.; He, X.; Wei, Z. Transient Localized Surface Plasmon Induced by Femtosecond Interband Excitation in Gold Nanoparticles. *Sci. Rep.* **2018**, *8* (1), 10499. https://doi.org/10.1038/s41598-018-28909-6.
(34) V. Hartland, G. Measurements of the Material Properties of Metal Nanoparticles by Time-Resolved Spectroscopy. *Phys. Chem. Chem. Phys.* **2004**, *6* (23), 5263–5274. https://doi.org/10.1039/B413368D.
(35) Chiang, W.-Y.; Bruncz, A.; Ostovar, B.; Searles, E. K.; Brasel, S.; Hartland, G.; Link, S. Electron–Phonon Relaxation Dynamics of Hot Electrons in Gold Nanoparticles Are Independent of Excitation Pathway. *J. Phys. Chem. C* **2023**, *127* (43), 21176–21185. https://doi.org/10.1021/acs.jpcc.3c04680.
(36) Hartland, G. V. Coherent Vibrational Motion in Metal Particles: Determination of the Vibrational Amplitude and Excitation Mechanism. *J. Chem. Phys.* **2002**, *116* (18), 8048–8055. https://doi.org/10.1063/1.1469021.

TOC Graphic: